NANO LETTERS

LETTER

pubs.acs.org/NanoLett

Interconnected Silicon Hollow Nanospheres for Lithium-Ion Battery Anodes with Long Cycle Life

Yan Yao,[†] Matthew T. McDowell,[†] Ill Ryu,[†] Hui Wu,[†] Nian Liu,[‡] Liangbing Hu,[†] William D. Nix,[†] and Yi Cui*[,†]

[†]Department of Materials Science and Engineering and [‡]Department of Chemistry, Stanford University, Stanford, California 94305, United States

Supporting Information

ABSTRACT: Silicon is a promising candidate for the anode material in lithium-ion batteries due to its high theoretical specific capacity. However, volume changes during cycling cause pulverization and capacity fade, and improving cycle life is a major research challenge. Here, we report a novel interconnected Si hollow nanosphere electrode that is capable of accommodating large volume changes without pulverization during cycling. We achieved the high initial discharge capacity of 2725 mAh g^{-1} with less than 8% capacity degradation every hundred cycles for 700 total cycles. Si hollow sphere electrodes also show a Coulombic efficiency of 99.5% in later cycles. Superior rate capability is demonstrated and attributed to fast lithium diffusion in the interconnected Si hollow structure.

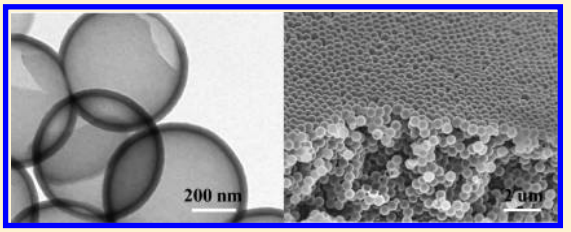

KEYWORDS: Silicon hollow sphere electrode, energy storage, lithium induced stress, volume expansion

The development of high-performance Li-ion batteries is critically important for use in portable electronics, electric vehicles, and the storage of renewable energy.[1,2] To meet these demanding applications, Li-ion batteries with high specific energy and long cycle life are required.[3] High specific energy can be achieved by utilizing electrode materials that have a higher specific capacity than current commercial electrode materials, and much research has been devoted to improving the performance and cycle life of high-capacity electrode materials.[4−8] One such material, silicon, reacts with lithium at low potentials and has 10 times greater theoretical specific capacity than graphite.[9−11] Unfortunately, the alloying reaction of Si with lithium causes significant volume expansion and results in particle fracture and loss of capacity with cycling.[12] One way that this issue has been addressed is to partially convert micrometer-sized crystalline Si particles to lithiated amorphous Si during initial conditioning cycles and then cycle with a lower voltage limit in the following cycles to maintain the two-phase lithiated amorphous/un-lithiated crystalline silicon structure.[13] This electrochemical conditioning method is promising, but limited capacities (960 mAh g^{-1}) have been exploited.[13]

Recently, Si nanostructures have been explored to attack the volume expansion and fracture problem. In previous work, we demonstrated Si nanowire electrodes that effectively address these problems; with these electrodes, the theoretical capacity of 4200 mAh g^{-1} could be reached.[6] We also explored core−shell crystalline/amorphous Si nanowires[14] and carbon/Si nanowires,[15] and we showed 90% capacity retention over 100 cycles. Cho et al. fabricated three-dimensional porous Si particles and demonstrated 2800 mAh g^{-1} capacity for 100 cycles.[16] Song et al. developed arrays of sealed Si nanotubes with 80% capacity retention after 50 cycles.[17] Yushin et al. reported Si/carbon composite porous particles (50 wt % of carbon) with 1950 mAh g^{-1} initial capacity and good cycling over 100 cycles.[18] For all these studies, the key design element is to have free volume around nanostructures so that they can expand without breaking. However, with this progress, a deeper understanding of volume expansion and stress evolution during the lithiation process in different types of nanostructures is important. Both theoretical modeling[19] and experimental in situ observation[20] can contribute to the understanding.

Here, we report an interconnected Si hollow nanosphere electrode that is capable of accommodating large strain without pulverization. Si hollow nanospheres serve as a simple model system for study due to their uniform size distribution compared to previously demonstrated nanostructures. We developed a finite element model to simulate the diffusion-induced stress evolution and investigated the volume expansion of the same single hollow spheres before and after lithiation using transmission electron microscopy. More interestingly, we achieved high initial discharge capacity of 2725 mAh g^{-1} and 700 cycles in electrochemical tests. Less than 8% capacity degrades for every 100 cycles. Even after 700 cycles, this Si hollow sphere electrode shows 1420 mAh g^{-1} capacity. Superior rate capability is demonstrated as well.

A number of recent models have been proposed to study stress evolution, diffusion, and fracture in battery materials.[19,21−23] We developed a finite element model to calculate the diffusion-induced stress during lithiation. In this model, the hollow

Received: May 3, 2011
Revised: June 1, 2011

   dx.doi.org/10.1021/nl201470j | *Nano Lett.* XXXX, XXX, 000–000

nanosphere is given mechanical properties of amorphous Si (Young's modulus of 80 GPa, Poisson's ratio of 0.22, yield stress of 1 GPa). The amorphous Si is modeled as elastically isotropic due to its amorphous nature. Since the volume expansion is significant, the effect of pressure gradient on Li flux needs to be considered. Adopting related analysis for spherical particles,[24,25] we rederive the stress relation for the hollow sphere geometry. From the analytical solution for the stress associated with the transformation strains,[26] the hydrostatic stress can be expressed by

$$\sigma_h(r) = \frac{1}{3}(\sigma_r + \sigma_\theta + \sigma_z) = \frac{2\Omega E}{9(1-\nu)}\left[\frac{3}{R^3 - a^3}\int_0^R C(r)r^2\,dr - C(r)\right] \quad (1)$$

where Ω is the partial molar volume of lithium and C is the concentration of lithium, E is Young's modulus, ν is the Poisson's ratio, R is the outer radius, and a is the inner radius of the hollow sphere.

The gradient of hydrostatic stress may be expressed as

$$\frac{\partial \sigma_h}{\partial r} = \frac{\partial}{\partial r}\left(\frac{2\Omega E}{9(1-\nu)}\left[\frac{3}{R^3 - a^3}\int_0^R C(r)r^2\,dr - C(r)\right]\right) = -\frac{2\Omega E}{9(1-\nu)}\frac{\partial c}{\partial r} \quad (2)$$

Substituting this expression into the diffusion equation, we get

$$\frac{\partial c}{\partial t} = D\left(\frac{\partial^2 c}{\partial r^2} + \frac{1}{r}\frac{\partial c}{\partial r} + \frac{2\Omega^2 E}{9RT(1-\nu)}\left(\frac{\partial c}{\partial r}\right)^2 + \frac{2\Omega^2 E c}{9RT(1-\nu)}\left(\frac{\partial^2 c}{\partial r^2} + \frac{1}{r}\frac{\partial c}{\partial r}\right)\right) \quad (3)$$

It turns out that this equation is the same as taking the diffusivity as a linear function of concentration

$$D = D(c) = \breve{D}(1 + \beta c) \quad (4)$$

where β can be expressed by

$$\beta = \frac{2\Omega^2 E}{9RT(1-\nu)} \quad (5)$$

Constant Li^+ ion flux charging conditions (C/10) are used as boundary conditions. A rate of C/10 corresponds to charging or discharging in 10 hours. When lithium diffuses into the hollow sphere, the outer part is lithiated first and expands but is constrained by the inner part of sphere which remains unlithiated. Thus the outer part will experience compressive hoop stress (defined as the stress in the plane perpendicular to the radial direction) and the inner part will experience tensile hoop stress. If a predefined crack exists, breaking will take place when the maximum tensile stress exceeds the critical value. Figure 1A plots the stress distribution across the shell cross section of a hollow sphere (R_{in} = 175 nm, R_{out} = 200 nm) and its evolution with time. Positive values indicate tensile stress, while negative values indicate compressive stress. The maximum tensile stress of 83.5 MPa develops at the inner surface after about 1 min of lithiation. Figure 1B plots the stress distribution across the cross section of a solid sphere (R = 138 nm) and its evolution with time. The maximum tensile stress of 439.7 MPa is generated in the center of the sphere after about 6 min of lithiation. Figure 1 shows that the maximum tensile stress in a hollow Si sphere is ~5 times lower than that in a solid sphere with an equal volume of Si (83.5 vs 439.7 MPa, respectively). This significant difference in the maximum tensile stress shows the unique advantage of a hollow sphere; these lower stress values mean that the hollow sphere will fracture less readily.

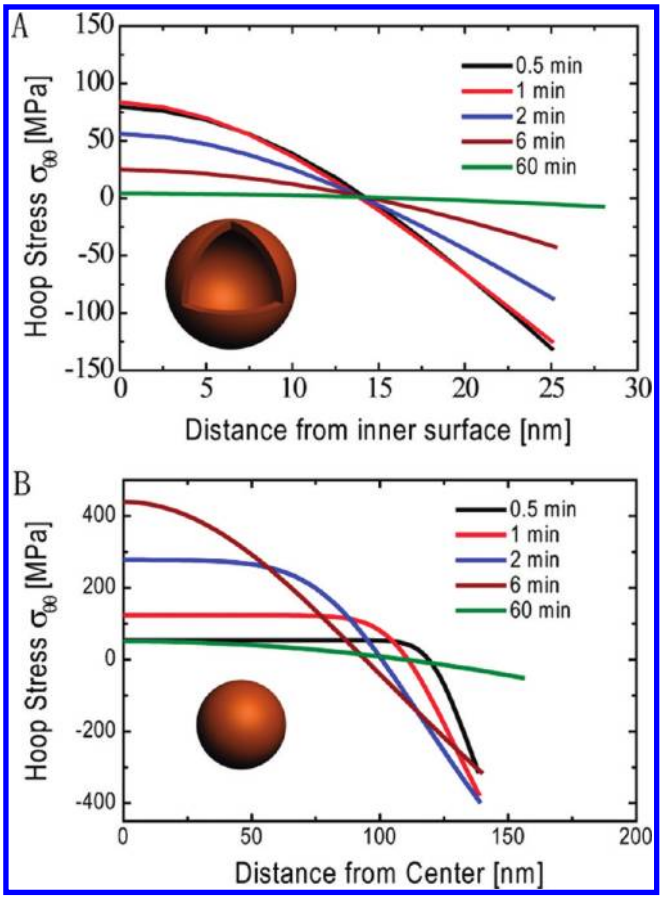

Figure 1. Theoretical modeling of stress evolution during lithiation in a hollow sphere vs a solid sphere with the same volume of Si. (A) Hoop stress ($\sigma_{\theta\theta}$) evolution of a hollow Si sphere at lithiation rate of C/10 for 0.5, 1, 2, 6, and 60 min. The inset shows a schematic of the hollow Si sphere (R_{in} = 175 nm, R_{out} = 200 nm). (B) Hoop stress ($\sigma_{\theta\theta}$) evolution of a solid Si sphere at at lithiation rate of C/10 for 0.5, 1, 2, 6, and 60 min. The inset shows a schematic of the solid Si sphere (R = 138 nm) that has the same volume of the hollow sphere. Positive stress value means tensile stress, while negative value means compressive stress.

To fabricate Si hollow nanosphere electrodes, we employed a template approach using solid silica nanospheres, as shown by the schematic in Figure 2A. First, monodisperse suspensions of colloidal silica particles with 350 nm diameter were prepared following the modified Stöber method;[27] these spheres were then drop-coated onto a stainless steel substrate. The thickness of this layer can be varied from 10 to 20 μm by the number of drop-coating steps. Next, an amorphous Si layer was deposited on the silica template by chemical vapor deposition (CVD) of SiH_4 at 485 °C for 20 min. Finally, the silica cores were removed by dilute HF etching. Figure 2B shows a typical cross-sectional scanning electron microscopy (SEM) image of an as-fabricated hollow Si sphere electrode; this image shows that the spheres are interconnected to form one piece with thickness ~12 μm.

dx.doi.org/10.1021/nl201470j |Nano Lett. XXXX, XXX, 000–000

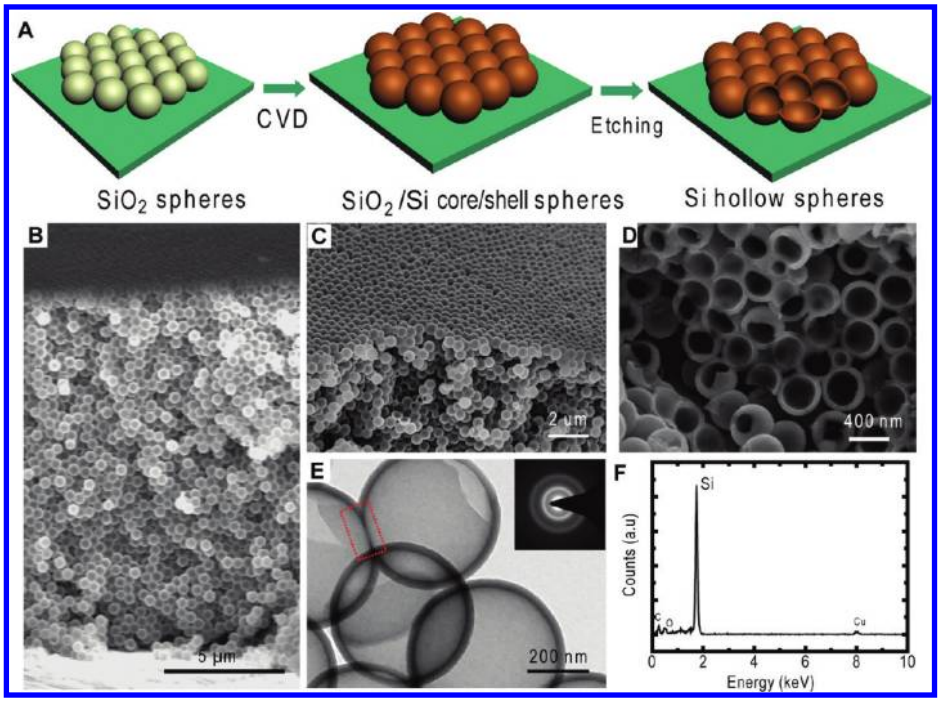

Figure 2. Synthesis and characterization of an interconnected Si hollow nanosphere electrode. (A) Schematic of hollow sphere synthesis. Silica particles ($R \sim 175$ nm) are first coated onto a stainless steel substrate, followed by CVD deposition of Si. The SiO_2 core is then removed by HF etching. (B) Typical cross-sectional SEM image of hollow Si nanospheres showing the underlying substrate and the electrode thickness of ~12 μm. Magnified images (Supplementary Figure 1, Supporting Information) show that spheres throughout the thickness of the electrode are all similar. (C) SEM side view (45° tilt) of the same sample of hollow Si nanospheres. (D) SEM image of hollow Si nanospheres scraped using a sharp razor blade, revealing the interior empty space in the spheres. (E) TEM image of interconnected hollow Si spheres ($R_{in} \sim 175$ nm, $R_{out} \sim 200$ nm). The area outlined by red dotted line indicates a shared shell between two interconnected spheres. Inset, the selected area electron diffraction pattern shows the amorphous nature of the sample. (F) Energy dispersive X-ray spectroscopy (EDS) of a hollow Si sphere. The carbon and copper signals come from the holey carbon TEM grids.

Higher-magnification SEM images in Figure S1 (Supporting Information) show that magnified spheres at the top, middle, and bottom parts of the electrode are all similar. The side-view SEM image of the same sample in Figure 2C shows the regular closed packed arrangement of spheres on the top surface.

To observe the vacant inner space in the spheres, samples were scraped using a sharp razor blade. The SEM image in Figure 2D clearly shows the inner and outer surfaces of hollow spheres, which are actually interconnected through shared shells. The transmission electron microscopy (TEM) image in Figure 2E further confirms the structure; the spheres have an inner radius (R_{in}) of ~175 nm and an outer radius (R_{out}) of ~200 nm. R_{in} is similar to that of the initial silica spheres. The area outlined by red lines indicates a shared shell between two interconnected spheres. Since we start from densely packed silica spheres, amorphous Si is deposited as a conformal coating on the surface of the spheres except in those areas where two silica spheres are in close contact. When HF is used to etch the SiO_2 template, HF solution flows through these contact points to neighboring spheres and results in holes on the shell (Figure 2C,E), thus forming an interconnected network. The selected area electron diffraction pattern in Figure 2E and the energy dispersive X-ray spectroscopy (EDS) data in Figure 2F confirm that the hollow spheres are composed of amorphous Si (the Cu and carbon signals come from the holey carbon TEM grid).

To investigate the electrochemical performance of hollow Si spheres, two-electrode 2032 coin cells with hollow Si sphere anodes ($R_{in} \sim 175$ nm, $R_{out} \sim 200$ nm) were fabricated with Li metal as the counter electrode. To investigate the intrinsic properties of the hollow Si nanospheres, galvanostatic cycling was used with voltage cutoffs of 0.01 and 1 V vs Li/Li^+. Figure 3A shows the voltage profiles of a hollow sphere anode for the first, second, 100th, and 500th galvanostatic charge/discharge cycles. For the first cycle at a rate of C/10, the charge and discharge capacities reach 3544 and 2725 mAh g^{-1}, and the Coulombic efficiency (CE) is 77%. In the following cycles, a rate of C/2 was used. The capacity at the 100th and 500th cycle, compared to the second cycle at the same rate, was 74% and 60%, respectively. The fact that the capacity only degrades 8% per 100 cycles over 700 total cycles indicates the superior stability of the hollow sphere electrode. The reversible Li discharge capacity and the Coulombic efficiency of the hollow Si nanospheres versus cycle number are plotted in Figure 3C. The Coulombic efficiency increases to 99% after 20 cycles and stabilizes at 99.5% in later cycles. Even at the 700th cycle, the discharge capacity is still 1420 mAh g^{-1}, which is 3.8 times that of the theoretical capacity of a graphite anode (372 mAh g^{-1}).

Figure 3B shows a typical cyclic voltammetry (CV) curve of the hollow Si nanosphere electrode over the potential window of 0.01−1 V at a scan rate of 0.1mVs^{-1} after the first cycle. The cathodic branch (Li alloy) shows two peaks at 0.07 and 0.21 V, which are attributed to the formation of an amorphous Li_xSi phase.[28] In the anodic branch (Li dealloy) the two peaks at 0.29 and 0.49 V correspond to de-lithiation back to amorphous Si.[28] The peaks and shape of the CV curve are consistent with the results previously reported in the literature for Si electrodes.[14,29,30] Figure 3D shows the charge/discharge capacities of the Si hollow spheres at 0.2, 1, 2, 5, and

dx.doi.org/10.1021/nl201470j |Nano Lett. XXXX, XXX, 000–000

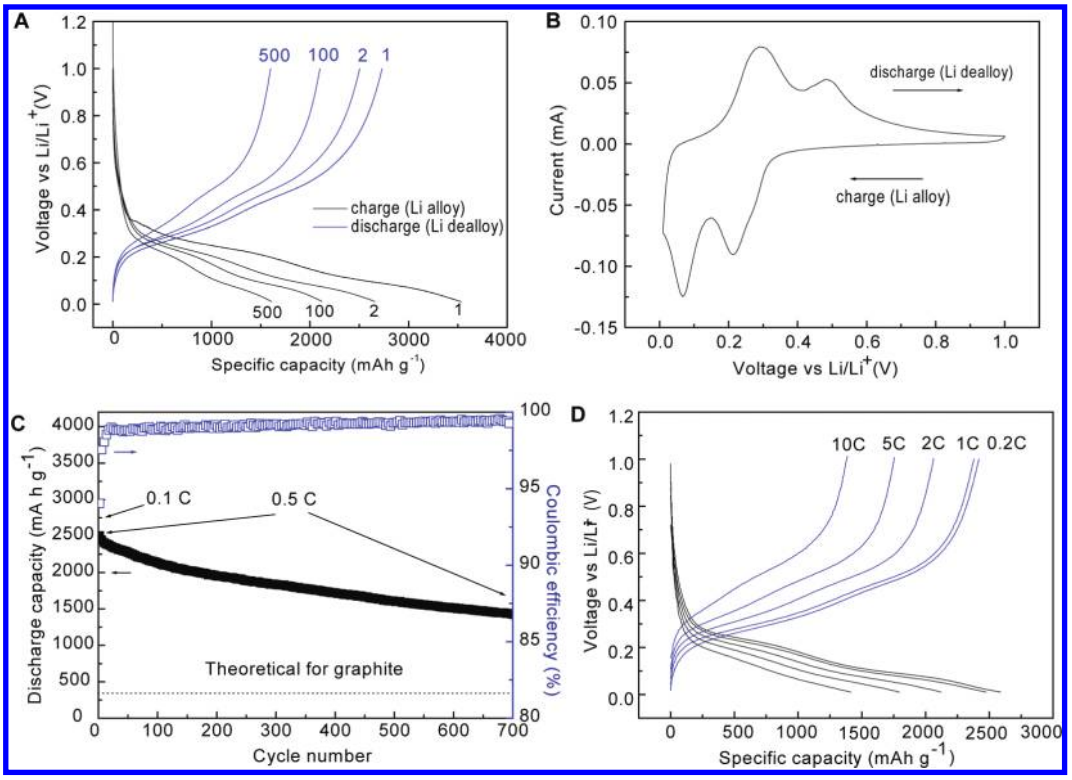

Figure 3. Electrochemical performance of interconnected Si hollow nanosphere electrodes (R_{in} ~ 175 nm, R_{out} ~ 200 nm). (A) Galvanostatic charge−discharge profiles between 0.01 and 1 V vs Li/Li^+ for the 1st, 2nd, 100th, and 500th cycles at a rate of 0.5 C, with the first cycle performed at 0.1 C. (B) Cyclic voltammetry curves of the second cycle of the hollow Si nanosphere electrode in the potential window between 0.01 to 1 V at a rate of 0.1 mV s^{-1}. (C) Reversible Li discharge capacity and Coulombic efficiency of the hollow Si nanospheres versus cycle number in comparison with the theoretical capacity of graphite. The discharge capacity degrades 8% per 100 cycles during the 700 total cycles. (D) Galvanostatic charge/discharge curves of Si hollow spheres electrode sequentially cycled at 0.2, 1, 2, 5, and 10 C rates with voltage cutoffs of 0.01 and 1 V. All measurements were carried out at room temperature in two-electrode 2032 coin-type half cells and no special cycling procedure was used.

10 C rates, at the current density of 0.44, 2.2, 4.4, 7.8, 14 A/g, respectively. The discharge (Li dealloying) capacities at these rates were 2417, 2378, 2060, 1756, and 1387 mAh g^{-1}, respectively. The discharge capacities at 2 and 5 C, compared to 0.2 C, were 85 and 73%, respectively. Even at 10 C, 57% of the 0.2 C capacity remained, with the voltage profile in the typical shape of amorphous Si. These high-rate capacity values are among the highest reported for silicon electrodes, and such a superior rate capability can be attributed to short lithium diffusion distance in the Si hollow shell.

To explore the volume changes in hollow Si spheres during reaction with Li, we used ex situ TEM to examine a set of the same spheres before and after lithiation. The spheres were placed on a conventional amorphous carbon TEM grid that had been coated with 20 nm of Ti; this was then inserted directly in a half-cell for reaction with Li by sweeping the voltage to 10 mV and holding for 24 h. TEM images of the same hollow spheres before (Figure 4A) and after (Figure 4B) lithiation reveal that the spheres undergo isotropic volume expansion. In this sphere, the inner radius R_{in} increases from ~175 to ~191 nm after lithiation, the shell thickness increases from ~25 to ~46 nm, and the outer radius increases from ~200 to ~237 nm. This results in a 240% volume expansion, and no fracture of the hollow spheres was observed. TEM images at lower magnification show that all connected spheres expand in a similar manner (see Figure S2, Supporting Information). This indicates that anodes made from hollow spheres can withstand volume expansion and could be an effective platform for enabling long cycle life. SEM was also used to monitor changes in morphology before (Figure 4C) and after 40 cycles (Figure 4D) and 700 cycles (Figure 4E) for different samples fabricated under the same condition. The surface of the hollow spheres becomes rough after 40 cycles, but the spheres are still intact even after 700 cycles.

The interconnected Si hollow nanosphere electrode has several advantages as an anode. First, the maximum tensile stress is greatly reduced compared to solid spheres; thus the hollow spheres are capable of accommodating large volume expansion without breaking. Second, the spheres are naturally interconnected, which eliminates the need for binders and Super P carbon black additives that normally constitute up to 20% of the weight in typical Si powder electrodes[31−33] and do not contribute to the total capacity. Third, R_{in} and R_{out} of the hollow spheres can be precisely controlled by the initial size of the silica spheres and the CVD deposition parameters, such as time and temperature. Shell thicknesses of tens of nanometers enable fast lithium diffusion and high rate capability. The combination of these factors indicates that this geometry is promising for use in Li-ion battery anodes. We note Ozin et al. explored inverse-opal structure Si electrodes using a similar template approach and demonstrated good capacity and cycling performance.[30] Compared to existing Si nanostructure anodes, such as crystalline nanowires[6] and nanoparticles,[34] the major improvement of Si hollow nanosphere electrodes comes from significantly reduced diffusion-induced stress due to the hollow nature of the structure. We recently

dx.doi.org/10.1021/nl201470j |Nano Lett. XXXX, XXX, 000–000

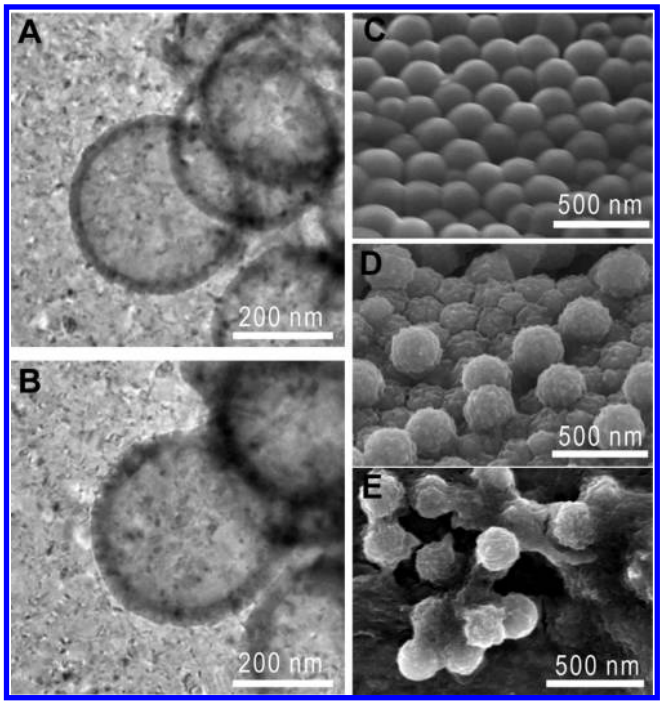

Figure 4. Tracking the volume changes in hollow Si nanospheres after lithiation with TEM and SEM. A conventional amorphous carbon TEM grid with reference marks coated with 20 nm of evaporated Ti was used. After initial imaging (A) in the TEM, the grids with hollow nanospheres were used directly as the working electrode in a half cell and were lithiated by sweeping the current from open circuit voltage to 10 mV at a rate of 0.1 mV/s; the electrodes were then held at 10 mV for 24 h. The grid was removed from the cell in an Ar glovebox, washed with acetonitrile, and the same hollow spheres were imaged again (B). SEM images of different hollow Si sphere samples fabricated under the same conditions: (C) before cycling, (D) after 40 cycles, and (E) after 700 cycles.

studied the critical size of Si NWs and found Si NWs prone to fracture when the diameter is larger than 300 nm.[35] In contrast, the hollow Si nanospheres shown in Figure 4, with outer diameter of 350 nm, still remain intact after full lithiation. The improved capacity retention may also due to reduced solid−electrolyte interphase (SEI) formation compared to smaller size solid Si nanoparticles. Aurbach et al. reported that the irreversible capacity of the nanoparticles is closely related to the intensive side reactions between the active material and electrolyte.[36] The hollow spheres have a free surface on the inside of the structure that is ideally not exposed to electrolyte. Compared to nanoparticles 10 nm in size that could have similar reduced stress values,[34] the hollow sphere geometry results in 85% less surface area exposed to the electrolyte for an equal volume of Si. This would decrease the significance of side reactions and SEI formation. Better control of SEI formation and disruption in our hollow nanospheres is expected to further improve the cycle stability.

In conclusion, we report the modeling, synthesis, and characterization of interconnected silicon hollow nanospheres as anodes in lithium-ion batteries. As an ideal model system, finite element modeling and ex situ TEM observation lead us to a deeper understanding of the volume expansion and stress evolution during the lithiation process. This study reports high capacity over 700 cycles, which is the longest ever reported for the silicon anode. These results suggest that the interconnected hollow nanosphere architecture is effective for mitigating the effects of volume expansion/contraction and represents a promising direction for use in practical batteries.

■ ASSOCIATED CONTENT

Supporting Information. Additional details on synthesis and characterization of interconnected Si hollow nanosphere electrodes. This material is available free of charge via the Internet at http://pubs.acs.org.

■ AUTHOR INFORMATION

Corresponding Author

*E-mail: yicui@stanford.edu.

Author Contributions

Y.Y. and Y.C. conceived of the idea. Y.Y., H.W., N.L., and L.H. performed the synthesis and cell fabrication, electrochemical tests, and characterization. M.T.M. performed TEM measurements. I.R. and W.D.N. carried out the mechanical modeling and analyzed data. Y.Y., M.T.M, and Y.C. cowrote the paper. All authors discussed the results and commented on the manuscript.

■ ACKNOWLEDGMENT

This work was partially supported by the Assistant Secretary for Energy Efficiency and Renewable Energy, Office of Vehicle Technologies of the U.S. Department of Energy under Contract No. DE-AC02-05CH11231, Subcontract NO. 6951379 under the Batteries for Advanced Transportation Technologies (BATT) Program. This work is also partially supported by the Department of Energy, Office of Basic Energy Sciences, Division of Materials Sciences and Engineering, under Contract DE-AC02-76SF0051, through the SLAC National Accelerator Laboratory LDRD project. Y.C. acknowledges support from the King Abdullah University of Science and Technology (KAUST) Investigator Award (No. KUS-l1-001-12). W.D.N and I.R. were supported by the Office of Science, Office of Basic Energy Sciences, of the US Department of Energy under Contract No. DE-FG02-04ER46163. M.T.M. gratefully acknowledges support from the Chevron Stanford Graduate Fellowship, the National Defense Science and Engineering Graduate Fellowship, and the National Science Foundation Graduate Fellowship.

■ REFERENCES

(1) Armand, M.; Tarascon, J. M. *Nature* **2008**, *451*, 652–657.
(2) Kang, B.; Ceder, G. *Nature* **2009**, *458*, 190–193.
(3) Whittingham, M. S. *MRS Bull.* **2008**, *33*, 411–419.
(4) Taberna, L.; Mitra, S.; Poizot, P.; Simon, P.; Tarascon, J. M. *Nat. Mater.* **2006**, *5*, 567–573.
(5) Ji, X. L.; Lee, K. T.; Nazar, L. F. *Nat. Mater.* **2009**, *8*, 500–506.
(6) Chan, C. K.; Peng, H. L.; Liu, G.; McIlwrath, K.; Zhang, X. F.; Huggins, R. A.; Cui, Y. *Nat. Nanotechnol.* **2008**, *3*, 31–35.
(7) Oumellal, Y.; Rougier, A.; Nazri, G. A.; Tarascon, J. M.; Aymard, L. *Nat. Mater.* **2008**, *7*, 916–921.
(8) Sun, Y. K.; Myung, S. T.; Park, B. C.; Prakash, J.; Belharouak, I.; Amine, K. *Nat. Mater.* **2009**, *8*, 320–324.
(9) Poizot, P.; Laruelle, S.; Grugeon, S.; Dupont, L.; Tarascon, J. M. *J. Power Sources* **2001**, *97−8*, 235–239.

(10) Kasavajjula, U.; Wang, C. S.; Appleby, A. J. *J. Power Sources* **2007**, *163*, 1003–1039.
(11) Choi, N.-S.; Yao, Y.; Cui, Y.; Cho, J. *J. Mater. Chem.* Submitted.
(12) Huggins, R. A. *J. Power Sources* **1999**, *81−82*, 13–19.
(13) Obrovac, M. N.; Krause, L. J. *J. Electrochem. Soc.* **2007**, *154*, A103–A108.
(14) Cui, L. F.; Ruffo, R.; Chan, C. K.; Peng, H. L.; Cui, Y. *Nano Lett.* **2009**, *9*, 491–495.
(15) Cui, L. F.; Yang, Y.; Hsu, C. M.; Cui, Y. *Nano Lett.* **2009**, *9*, 3370–3374.
(16) Kim, H.; Han, B.; Choo, J.; Cho, J. *Angew. Chem., Int. Ed.* **2008**, *47*, 10151–10154.
(17) Song, T.; Xia, J. L.; Lee, J. H.; Lee, D. H.; Kwon, M. S.; Choi, J. M.; Wu, J.; Doo, S. K.; Chang, H.; Il Park, W.; Zang, D. S.; Kim, H.; Huang, Y. G.; Hwang, K. C.; Rogers, J. A.; Paik, U. *Nano Lett.* **2010**, *10*, 1710–1716.
(18) Magasinski, A.; Dixon, P.; Hertzberg, B.; Kvit, A.; Ayala, J.; Yushin, G. *Nat. Mater.* **2010**, *9*, 353–358.
(19) Christensen, J.; Newman, J. *J. Solid State Electrochem.* **2006**, *10*, 293–319.
(20) Sethuraman, V. A.; Chon, M. J.; Shimshak, M.; Srinivasan, V.; Guduru, P. R. *J. Power Sources* **2010**, *195*, 5062–5066.
(21) Bower, A. F.; Guduru, P. R.; Sethuraman, V. A. *J. Mech. Phys. Solids* **2011**, *59*, 804–828.
(22) Zhao, K. J.; Pharr, M.; Vlassak, J. J.; Suo, Z. G. *J. Appl. Phys.* **2010**, 108.
(23) Cheng, Y. T.; Verbrugge, M. W. *J. Power Sources* **2009**, *190*, 453–460.
(24) Zhang, X.; Shyy, W.; Sastry, A. M. *J. Electrochem. Soc.* **2007**, *154*, A910–A916.
(25) Woodford, W. H.; Chiang, Y. M.; Carter, W. C. *J. Electrochem. Soc.* **2010**, *157*, A1052–A1059.
(26) Timoshenko, S. P.; Goodier, J. N. *Theory of Elasticity*, 3rd ed.; McGraw-Hill: NewYork, 1970.
(27) Stober, W.; Fink, A.; Bohn, E. *J. Colloid Interface Sci.* **1968**, *26*, 62-&.
(28) Li, J.; Dahn, J. R. *J. Electrochem. Soc.* **2007**, *154*, A156–A161.
(29) Chan, C. K.; Ruffo, R.; Hong, S. S.; Huggins, R. A.; Cui, Y. *J. Power Sources* **2009**, *189*, 34–39.
(30) Esmanski, A.; Ozin, G. A. *Adv. Funct. Mater.* **2009**, *19*, 1999–2010.
(31) Magasinski, A.; Zdyrko, B.; Kovalenko, I.; Hertzberg, B.; Burtovyy, R.; Huebner, C. F.; Fuller, T. F.; Luzinov, I.; Yushin, G. *ACS Appl. Mater. Interfaces* **2010**, *2*, 3004–3010.
(32) Li, J.; Lewis, R. B.; Dahn, J. R. *Electrochem. Solid-State Lett.* **2007**, *10*, A17–A20.
(33) Xiao, J.; Xu, W.; Wang, D.; Choi, D.; Wang, W.; Li, X.; Graff, G. L.; Liu, J.; Zhang, J.-G. *J. Electrochem. Soc.* **2010**, *157*, A1047–A1051.
(34) Kim, H.; Seo, M.; Park, M. H.; Cho, J. *Angew. Chem., Int. Ed.* **2010**, *49*, 2146–2149.
(35) Ryu, I.; Choi, J. W.; Cui, Y.; Nix, W. D. *J. Mech. Phys. Solids*, in press.
(36) Aurbach, D.; Nimberger, A.; Markovsky, B.; Levi, E.; Sominski, E.; Gedanken, A. *Chem. Mater.* **2002**, *14*, 4155–4163.